Electrochemical and Solid-State Letters, **9** (8) A373-A375 (2006)
1099-0062/2006/9(8)/A373/3/$20.00 © The Electrochemical Society

SnO_2 Filled Mesoporous Tin Phosphate

High Capacity Negative Electrode for Lithium Secondary Battery

Jinyoung Kim and Jaephil Cho*,z

Department of Applied Chemistry, Kumoh National Institute of Technology, Gumi, Korea

SnO_2 filled mesoporous tin phosphate was prepared by impregnating an Sn melt into the mesopores of hexagonal mesoporous tin phosphate with a pore size of 3 nm at 300°C under vacuum. Although Sn was oxidized to SnO_2 via a reaction with the oxygen ions consisting of one of tin phosphate pore wall frameworks at 300°C, the pore wall material remained amorphous without showing any other phases. The electrochemical results revealed significant improvement of the reversible capacity to 805 from 400 mAh/g after the mesopores were filled with SnO_2. This was because the SnO_2 not only added capacity but also decreased high BET surface area of the mesoporous tin phosphate that caused the large irreversible capacity.
 [DOI: 10.1149/1.2205119]

Manuscript submitted February 13, 2006; revised manuscript received March 21, 2006. Available electronically May 23, 2006.

Mesoporous materials have been investigated extensively due to their potential applications as catalysts, electrical insulators, and optics.[1-6] On the other hand, their applications to electrode materials in lithium secondary batteries have received little attention because of the very limited candidates.[7,8] Recently, it was reported that mesoporous tin phosphate composites showed reversible pore expansion and contraction during lithium alloying and dealloying.[9,10] These pores act as a buffer layer to accommodate the volume changes in the pore wall frameworks. In spite of this advantage, mesoporous tin phosphate composites exhibit a low specific capacity (<500 mAh/g) and large irreversible capacity (>200%) due to the large Brunauer-Emmett-Teller (BET) surface area, which leads to enhanced side reactions at the interfaces between the electrolyte and electrode.[10] In addition, this material showed a low electrode density due to the larger pore fraction than other electrode materials. Therefore, the best way to reduce the irreversible capacity and at the same time increase the electrode density is to fill the empty mesopores with a metal or metal oxide. The filling material can be expected to give additional capacity if it is lithium reactive.

There have been several studies reported on the metal or metal oxide (nanosized ZnS, Au, Pt, or Ga) confined nanotubes or mesoporous materials even though these are for catalytic applications.[11-17] These materials were prepared by either ion-exchange of the metals into the matrix phases followed by reduction or metal impregnation into the mesoporous materials by controlling the particle size. In the first case, metal atoms are initially generated adjacent to the ion exchange position of the framework and form clusters on the outer surface. As long as the size of the cluster is smaller than the pore, it can be encapsulated in the pore system. However, the distribution of particles is generally not uniform and a metal component can be found both inside the pores and on the outer surface. On the other hand, the latter method rarely gives a uniform distribution of metal particles as long as the particle size is smaller than the pore size. Recently, tin filled carbon and SnO_2-mesoporous carbon composites were used as possible negative electrode materials for Li secondary batteries but they showed a large irreversible capacity over 100%.[14,17] This is due to the large BET surface area of the supported carbon nanotubes.

In this study, hexagonal mesopores with a 3 nm pore size in mesoporous tin phosphate were filled with SnO_2 by melting Sn at 300°C. Because Sn metal is tuned into a completely fluid-like liquid at 300°C,[18] it can be easily impregnated into the mesopores.

Experimental

For preparing tin metal nanoparticles, 0.7 mmol of tetraoctylammonium bromide as a catalyst was added to $SnCl_4 \cdot 5H_2O$ (0.9 mmol) in a solution of 15 mL CH_2Cl_2 and deionized, deoxygenized water with vigorous stirring. A solution of 3-(2-pyridyl)-5,6-diphenyl-1,2,4-triazine (capping agent) with 4.8 mmol in 100 mL of CH_2Cl_2 was added, and the resulting solution was stirred at room temperature for 20 min. $NaBH_4$, as a reducing agent, (18 mmol) in 20 mL of deionized water was then added.[19] The mixture was stirred for 1 h at room temperature under an argon atmosphere. After the reaction, the mixture was washed four times with water and acetone and vaporated in vacuo to yield the tin particles. Mesoporous tin phosphate was prepared by mixing 3 g of SnF_2 and 8.8 g of H_3PO_4, followed by dissolving in 10 mL of distilled-deionized water (DDW). 0.0095 mol of alkyltrimethylammonium bromide $CH_3(CH_2)_nN(CH_3)_3Br$ surfactant was then dissolved in 10 mL of DDW, and the resulting solution was added to the solution of $SnCl_2 \cdot H_2O$ and H_3PO_4. The resulting mixture was stirred at 40°C for 1 h, and loaded in an autoclave, followed by heating at 70 and 90°C for 5 and 15 h, respectively. After cooling to room temperature, the precipitate was recovered by filtration, washed with distilled water, and vacuum-dried at 100°C for 10 h. The as-prepared mesoporous tin phosphate powders were then annealed at 400°C for 3 h, yielding mesoporous tin phosphate.

To prepare the SnO_2-filled sample, as-prepared both tin nanoparticles and mesoporous tin phosphate in a weight ratio of 4:6, 5:5, and 6:4 (Sn:mesoporous tin phosphate) were thoroughly mixed using a magnetic bar in an ethanol solution for 30 min and vacuum-dried at 100°C. This was followed by heat-treatment at 300°C for 0.4 h under vacuum (Figs. 1). A direct reaction between Sn and tin phosphate occurred at 300°C after 2 h or at 400°C, resulting in the formation of a crystalline $Sn_2P_2O_7$ phase.

SnO_2 nanoparticles with an average size of ~2.5 nm were synthesized from $SnCl_4$ and triethylenediamine (TEDA: $C_6H_{12}N_2$), as a capping agent, using the hydrothermal method.[20] $SnCl_4$ (1 g) was first dissolved in 50 mL of distilled water, followed by the addition of 0.7 g TEDA under magnetic stirring. The mixture was then transferred into a Teflon-lined stainless steel autoclave and maintained at 110°C, for ~20 h.

The electrochemical studies were carried out using coin-type half cells (2016 type) with a Li counter electrode. Sn nanoparticle: binder: carbon black in a weight ratio of 8:1:1 was used as the

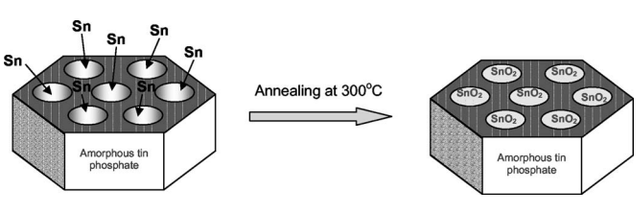

Figure 1. Schematic diagram of the SnO_2-filled mesoporous tin phosphate via the Sn melt impregnation method.

* Electrochemical Society Active Member.
z E-mail: jpcho@kumoh.ac.kr

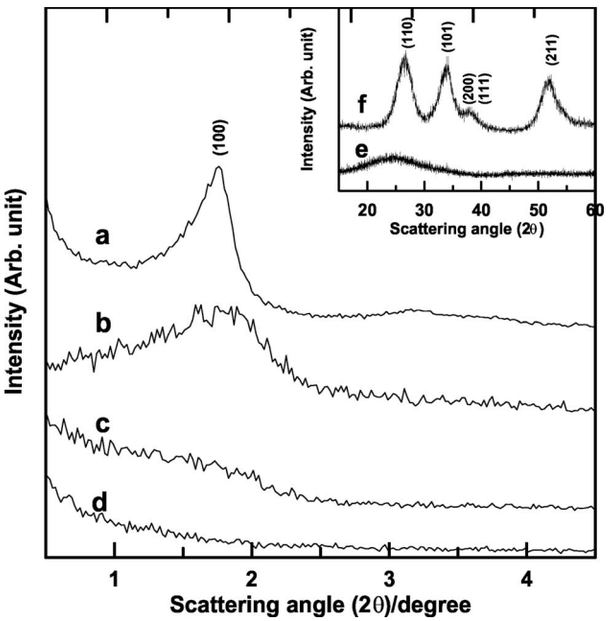

Figure 2. Small angle XRD patterns of (a) as-prepared mesoporous tin phosphate and tin impregnated mesoporous tin phosphate in a different weight ratio of (b) 6:4, (c) 5:5, and (d) 4:6 (meso: tin impregnated). Insets (e) and (f) are wide angle XRD patterns of (a) and (d), respectively.

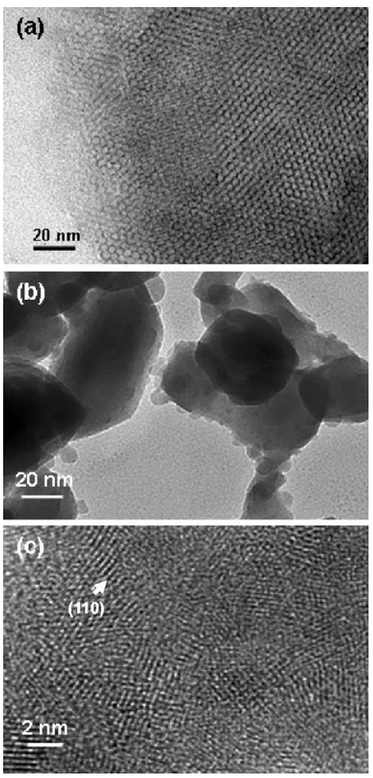

Figure 3. TEM images of (a) as-prepared mesoporous tin phosphate, (b) SnO_2-filled, and (c) magnified image of (b).

working electrode. The working electrode was made from the active material, Super P carbon black (MMM, Belgium), and polyvinylidene fluoride (PVdF) binder (Solef, Belgium). The small-angle X-ray scattering (SAXS) patterns were obtained using Cu Kα radiation (40 kV, 35 mA) with a Bruker Nanostar. Nitrogen adsorption isotherm was measured at 77 K on a Micromeritics ASAP 2010 gas sorption system.

Results and Discussion

Figure 2a shows the SAXS patterns of the mesoporous tin phosphate before and after annealing (400°C for 3 h). The strong peak indexed as (100) confirms the ordered hexagonal mesostructure.[21,22] The corresponding *d* spacing of the as-synthesized mesoporous tin phosphate is 5.0 ± 0.2 nm. The high-angle X-ray diffraction (XRD) pattern (the inset of Fig. 2e) showed broad peaks with weak intensities, indicating that the tin phosphate consisted of amorphous or nanocrystalline mesoporous walls.[23,24] Figure 3a shows a transmission electron microscopy (TEM) image of the sample, clearly indicating the presence of a hexagonal mesostructure. The corresponding spacing by TEM is ~5 nm, which is consistent with the SAXS data. Figure 4 shows the N_2 adsorption isotherm of the annealed sample, and the BET surface area is ~185 m^2/g. The measured BET surface area is in good agreement with that reported for other nonsiliceous mesoporous solids.[13,25] The average pore size in the annealed sample (inset of Fig. 4) was ~3 nm (by the Barrett-Joyner-Halenda analysis), which is consistent with the SAXS and TEM (Fig. 2 and 3 respectively).

Figures 2b-d show the SAXS patterns of tin impregnated mesoporous tin phosphate in a different weight ratio of 6:4, 5:5, and 4:6 (meso: tin impregnated). As the weight ratio of tin was increased, peak intensity of the mesopore structure decreased and completely disappeared at a weight ratio of 4:6. This indicates that the mesopores were filled with Sn metals. However, the wide angle XRD pattern of the sample with a 4:6 ratio (Fig. 2f) shows the presence of SnO_2. The formation of SnO_2 phase is due to a reaction between Sn and oxygen ions of the pore wall tin phosphate phase at 300°C. However, the possibility of a partial reaction between Sn and tin phosphate phase at the interface cannot be ruled out. The particle size was estimated to be ~3 nm. Considering the pore wall size of 3 nm, the estimated SnO_2 particle size is in good agreement with the mesopore size, indicating that most of the tin oxide was confined in the mesopores. On the other hand, we did not find other tin phosphate peaks in the XRD pattern (Fig. 2f), indicating that this phase remains as an amorphous or nanocrystalline phase. Figures 3b and c show TEM images of the SnO_2-filled sample and its expanded one,

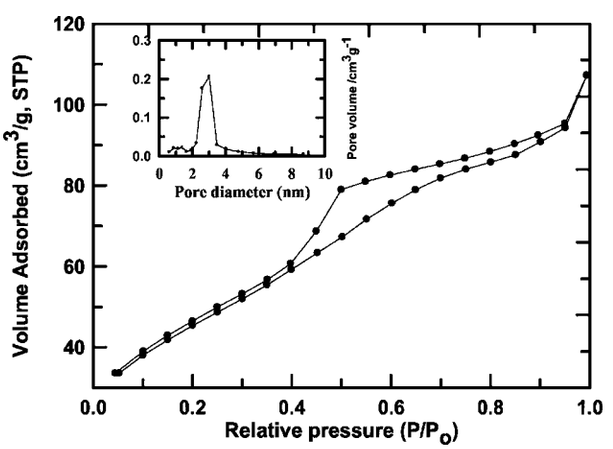

Figure 4. Representative nitrogen adsorption and desorption isotherms of SnO_2-filled tin phosphate. The corresponding BJH distribution is shown in the inset.

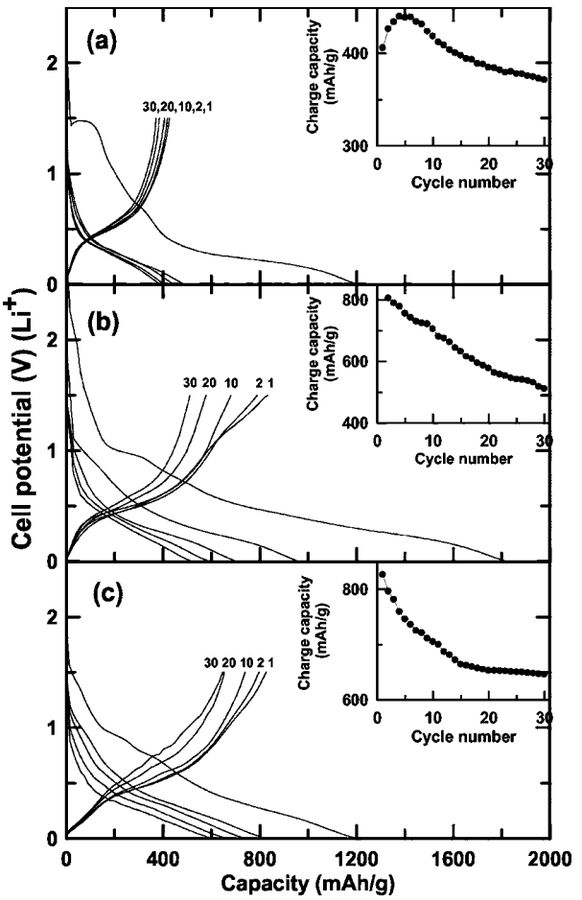

Figure 5. Voltage profiles of (a) mesoporous tin phosphate, (b) SnO_2 nanoparticles, and (c) SnO_2-filled nanoparticles in coin-type half-cells. The anodes were cycled at a rate of 200 mA/g between 1.5 and 0 V.

respectively. The mesopores were covered by the SnO_2 phase; the lattice fringes of tetragonal SnO_2 corresponding to the (200) plane are shown.

Figure 5 shows the voltage profiles of the mesoporous tin phosphate, SnO_2 nanoparticle ($\sim$3 nm), and SnO_2-filled mesoporous tin phosphate, along with the capacity retention as a function of the cycle number. Because of the high BET surface area of the mesoporous tin phosphate, the first discharge and charge capacities were 1119 and 419 mAh/g, respectively, with a very large irreversible capacity corresponding to 267% of the charge capacity. Its capacity retention was 89% after 30 cycles. On the other hand, the nanosized SnO_2 showed a little smaller irreversible capacity than the mesoporous tin phosphate, showing 220% of the charge capacity (832 mAh/g). The capacity retention ratio after 30 cycles was 61% (511 from 831 mAh/g). A previous study showed that a 1.2 V cutoff of the $\sim$3 nm sized mesopores had no capacity fading, which was due to the lack of particle growth.[20] However, such capacity fading at a 1.5 V cutoff was due to the enhanced aggregation of the Sn particles into larger particles, resulting in pulverization and electric connectivity between the composite electrode components.[26,27]

Finally, the SnO_2-filled sample shows a much lower irreversible capacity than the mesoporous and SnO_2 samples, showing by 120 and 74%, respectively. The first discharge and charge capacities were 826 and 1204 mAh/g, respectively, showing a 69% reversible capacity ratio. Considering capacity from the mesoporous and SnO_2 composite only ($0.6 \times 832 + 0.4 \times 419 = 667$ mAh/g), SnO_2-filled sample should have been 667 mAh/g. However, the composite exhibits an additional capacity increase of 119 mAh/g. This might be due to the decreased BET surface area (30 m^2/g), resulting in a decreased surface reaction at the electrolyte/electrode interface. We expected that decreased surface area to 30 m^2/g from 180 m^2/g after SnO_2 filling may affect the rate capability. Comparison of rate capability at higher rates above 2C is underway using Li-ion cells. The capacity retention after 30 cycles was 78%, which corresponded to 28% improvement over that observed with SnO_2 nanoparticles. However, the slightly smaller capacity retention compared with mesoporous tin phosphate was attributed to the mesopores, which was acts as a buffer layer for the volume expansion, being completely blocked by SnO_2. In addition, capacity fading may be induced from that the surface covered SnO_2 particles which did not fill the mesopores were pulverized into smaller particles during cycling. We reported that irreversible capacity was also reduced by the amorphous carbon coating effectively.[28] However, the most effective way to both increase the electrode density and irreversible capacity is believed to filling the mesopores with SnO_2.

In conclusion, SnO_2-filled mesoporous tin phosphate exhibited a significantly lower irreversible capacity and relatively good capacity retention, compared with mesoporous tin phosphate and nanosized SnO_2 between 0 and 1.5 V. Moreover, the specific capacity of the SnO_2-filled anode was improved by 2 times larger than pure mesoporous tin phosphate.

Acknowledgment

This work was supported by Ministry of Commerce, Industry and Energy.

Kumoh National Institute of Technology assisted in meeting the publication costs of this article.

References

1. T. Sun and J. Y. Ying, *Nature (London)*, **389**, 704 (1997).
2. S. Inagaki, S. Guan, T. Ohsuna, and O. Terasaki, *Nature (London)*, **416**, 304 (2002).
3. J. Y. Ying, C. P. Mehnert, and M. S. Wong, *Angew. Chem., Int. Ed.*, **38**, 56 (1999).
4. K. G. Severin, T. M. Abdel-Fattah, and T. J. Pinnavia, *Chem. Commun. (Cambridge)*, **1998**, 1471.
5. T. Katou, B. Lee, D. Lu, J. N. Kondo, M. Hara, and K. Domen, *Angew. Chem., Int. Ed.*, **42**, 2382 (2003).
6. C. Serre, A. Auroux, A. Gervassini, M. Hervieu, and G. Ferey, *Angew. Chem., Int. Ed.*, **41**, 1594 (2002).
7. Z. Peng, Z. Shi, and M. Liu, *Chem. Commun. (Cambridge)*, **2000**, 2125.
8. F. Chen, Z. Shi, and M. Liu, *Chem. Commun. (Cambridge)*, **2000**, 2095.
9. E. Kim, M. G. Kim, Y. Kim, and J. Cho, *Electrochem. Solid-State Lett.*, **8**, A452 (2005).
10. E. Kim, D. Son, T.-G. Kim, J. Cho, B. Park, K. S. Ryu, and S. Chang, *Angew. Chem., Int. Ed.*, **43**, 5987 (2004).
11. W. C. Choi, S. I. Woo, M. K. Jeon, J. M. Sohn, M. R. Kim, and H. J. Jeon, *Adv. Mater. (Weinheim, Ger.)*, **17**, 446 (2005).
12. Z. Liu, Y. Bando, M. Mitome, and J. Zhan, *Phys. Rev. Lett.*, **93**, 095504 (2004).
13. J. Fan, T. Wang, C. Yu, B. Tu, Z. Jiang, and D. Zhao, *Adv. Mater. (Weinheim, Ger.)*, **16**, 1432 (2004).
14. K. Kim, S. H. Lee, W. Yu, J. Kim, J. W. Choi, Y. Park, and J. Jin, *Adv. Mater. (Weinheim, Ger.)*, **15**, 1618 (2003).
15. Y. Yang, J. Y. Lee, and H. C. Zeng, *Chem. Mater.*, **17**, 3899 (2005).
16. W. Zhang, J. Shi, H. Chen, and Zi. Hua, *Chem. Mater.*, **13**, 648 (2001).
17. T. P. Kumar, R. Ramesh, Y. Y. Lin, and G. T.-K. Fey, *Electrochem. Commun.*, **6**, 520 (2004).
18. *Encyclopedia of Chemistry*, 5th ed., G. D. Comsidine, Editor, John Wiley & Sons Inc., Hoboken, NJ (2005).
19. M. Noh, Y. Kim, M. G. Kim, H. Lee, H. Kim, Y. Kwon, Y. Lee, and J. Cho, *Chem. Mater.*, **17**, 3320 (2005).
20. C. Kim, M. Noh, M. Choi, J. Cho, and B. Park, *Chem. Mater.*, **17**, 3297 (2005).
21. G. Li, S. Bhosale, T. Wang, Y. Zhang, H. Zhu, and J.-H. Fuhrhop, *Angew. Chem., Int. Ed.*, **42**, 3818 (2003).
22. S.-H. Baeck, K.-S. Choi, T. F. Jaramillo, G. D. Stucky, and E. W. McFarland, *Adv. Mater. (Weinheim, Ger.)*, **13**, 11 (2001).
23. P. Yang, D. Zhao, D. I. Margolese, B. F. Chmelka, and G. D. Stucky, *Nature (London)*, **396**, 152 (1996).
24. D. Zhao, P. Yang, N. Melosh, J. Feng, B. F. Chmelka, and G. D. Stucky, *Adv. Mater. (Weinheim, Ger.)*, **10**, 1380 (1998).
25. F. Schüth, *Chem. Mater.*, **13**, 3184 (2001).
26. I. A. Courteny and J. R. Dahn, *J. Electrochem. Soc.*, **144**, 2045 (1997).
27. M. Winter and J. O. Besenhard, *Electrochim. Acta*, **45**, 31 (1999).
28. E. Kim, M. G. Kim, and J. Cho, *Electrochem. Solid-State Lett.*, **9**, A156 (2006).